Fines generation from South African manganese ores during preheating in a rotary kiln

by M.S. Moholwa[1,2], J.D. Steenkamp[1,3], and H.L. Rutto[2]

Affiliation:
[1] Mintek, Randburg, South Africa.
[2] Vaal University of Technology, Vanderbijlpark, South Africa.
[3] University of the Witwatersrand, Johannesburg, South Africa.

Correspondence to:
M. Moholwa

Email:
sammo@mintek.co.za

Dates:
Received: 30 Aug. 2021
Revised: 22 July 2022
Accepted: 30 July 2022
Published: November 2022

How to cite:
Moholwa, M.S., Steenkamp, J.D., and Rutto, H.L. 2022
Fines generation from South African manganese ores during preheating in a rotary kiln.
Journal of the Southern African Institute of Mining and Metallurgy, vol. 122, no. 11, pp. 629–638

DOI ID:
http://dx.doi.org/10.17159/2411-9717/1724/2022

Synopsis

Manganese ores are the major source of manganese for the production of manganese ferroalloys. There is a gap in the knowledge of the decrepitation behaviour of manganese ores, which presents a problem in the operation of smelters. Decrepitation, which is the breakage of the ore particles upon heating, is an important quality parameter for these ores. The purpose of this investigation was to determine the extent to which South African manganese ores decrepitate during preheating in a rotary kiln. The effects of temperature, rotational speed, and particle size decrepitation were investigated. Manganese ores were heated in a laboratory-scale rotary kiln at temperatures of 600, 800, and 1000°C, and rotational speeds of 3, 6, and 12 r/min. The size ranges were +6-20, +20-40, and +40-75 mm and the residence time was constant at 30 minutes. The decrepitation index (DI) is quantified as the ratio of the mass of <6 mm particles after pre-heating to the total mass of the sample. It was found that the DIs for all ores used were proportional to the temperature and the rotational speed and inversely proportional to the particle size range with temperature being the most important parameter. Ore A was the most susceptible to decrepitation followed by ore C and ore B; this was mainly to the decomposition of kutnohorite, the content of which was the highest in ore A and the lowest in ore B.

Keywords

decrepitation, manganese ores, rotary kiln, temperature, rotational speed, size range.

Introduction

Manganese ores are mostly used as a raw material in the production of manganese ferroalloys (Faria, Jannoti, and da Silva Araújo, 2012). Due to the desirable properties that manganese imparts to steel, the bulk of the ferromanganese alloys produced is consumed by the steel industry (Olsen, Tangstad, and Lindstad, 2007). There are 810 mt of total manganese reserves worldwide, and 83% of it is found in South Africa, the Ukraine, Australia, Brazil, and India (Sangine, 2020). The production of high-carbon ferromanganese (HCFeMn) is carried out mainly in submerged arc furnaces (SAFs) through the carbothermic reduction of manganese ores (Olsen, Tangstad, and Lindstad, 2007). The SAFs used in the production of HCFeMn are in general circular and have three graphite electrodes spaced equilaterally (Olsen, Tangstad, and Lindstad, 2007). The electrodes are submerged in the burden with an electric current running through the area below the electrode tips (Olsen, Tangstad, and Lindstad, 2007). The metal and slag are tapped either from the same tap-hole or separately from different slag and metal tap-holes (Olsen, Tangstad, and Lindstad, 2007). A cross-sectional view of the SAF is displayed in Figure 1.

The production of manganese in a submerged arc furnace is a highly energy-intensive process and releases large amounts of CO_2 gas (Olsen, Tangstad, and Lindstad, 2007). Emissions of CO_2 gas and shortage of energy are global problems, therefore there is a need to reduce energy consumption and CO_2 emissions from industrial processes (Pegels, 2010). PREMA is project that aims to demonstrate a suite of innovative technologies that involve the use of industrial off-gas and solar thermal energy

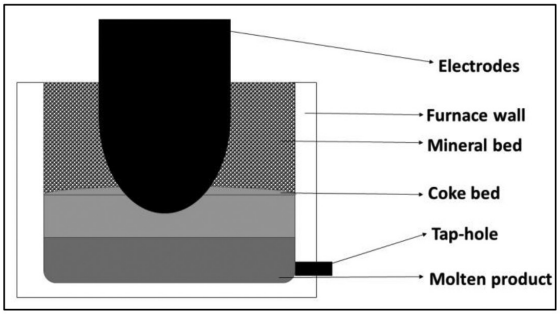

Figure 1—Cross-sectional view of a submerged arc furnace

to reduce energy consumption and emissions of CO_2 from the manganese production process (PREMA, 2019). PREMA proposed the incorporation of a pre-heating unit in the existing process of manganese production. The effect of preheating on the smelter is being investigated by Mintek in South Africa. A pilot-scale facility is being developed which includes a rotary kiln coupled to an alternating current (AC) submerged arc furnace. The use of a rotary kiln as a preheating unit necessitates the consideration of ore decrepitation during the rotation and heating of the of the ore in the kiln.

Decrepitation is the breakage of ore particles upon heating to produce fines (Faria *et al.*, 2013). The decrepitation index (DI) is used to evaluate the behaviour of lump ores when subject to heating and is defined by Equation [1]. The potential for decrepitation necessitated an investigation to determine to what extent South African manganese ores decrepitate during preheating. Fine particles resulting from decrepitation reduce the permeability of the burden, which will affect safety and efficiency of the SAF, and could lead to an eruption or explosion (Faria, Jannoti, and da Silva Araújo, 2012).

$$DI(< 6\ \text{mm}) = \left({}^{M1}/_{M2}\right) \text{X } 100 \qquad [1]$$

DI = Decrepitation index.
$M1$ = Mass of particles < 6 mm after heating (g).
$M2$ = Total mass of the sample after heating (g).

Decrepitation of manganese ores

Faria *et al.* (2012, 2013) have shown that the rate of decrepitation of Mn ores is influenced by a variety of factors. Mineralogical composition and physical properties are two such factors. The study by Faria, Jannoti, and da Silva Araújo, (2012) utilized four ores with different mineralogical compositions (Table I). The Azul and Urucum ores were mainly composed of oxides with a prevalence of cryptomelane. The Morro da Mina ore composed mainly of carbonates and silicates, while Wessels ore is comprised of braunite and carbonates. The study found that manganese oxides decrepitate mainly due to cryptomelane and pyrolusite decomposition during heating. Cryptomelane decomposes between 500°C and 900°C, while pyrolusite undergoes a phase transformation to bixbyite at 700°C (Biswas, Das, and Singh, 2016). Pyrolusite has a tetragonal crystal structure while bixbyite is isometric (Faria, Jannoti, and da Silva Araújo, 2012). The volumetric change associated with the phase change contributed to the decrepitation of Azul and Urucum ore.

The moisture content of the ores and the geometry of the crucibles used in the test affect the decrepitation of manganese ore (Biswas, Das, and Singh, 2016). The removal of structural water from the hydrated phases such as goethite (FeO(OH)) and clay minerals during heating contribute towards decrepitation (Biswas, Das, and Singh, 2016; Faria, Jannoti, and da Silva Araújo, 2012). Gradual heating eliminates thermal shock which in turn reduces the decrepitation intensity (Faria, Jannoti, and da Silva Araújo, 2012).

Decrepitation in rotary kilns

Rotary kilns are industrial or laboratory-scale furnaces which are long and cylindrical and slightly tilted during operation (Pisaroni, Sadi, and Lahaye, 2012). Rotary kilns have a wide range of material processing applications, including cement production and sponge iron production. The tilting angle differs for different applications. The material being processed is fed into the upper end of the cylinder, leaving a considerable amount of freeboard or empty space. The material bed gradually moves down towards the lower end as the kiln rotates about its axis. This rotation and downward movement promote a certain amount of stirring and mixing (Pisaroni, Sadi, and Lahaye, 2012). A tumbler is basically a rotary kiln without the heating elements, hence the factors that cause fines generation in the tumbler will represent fines generation in rotary kilns (Kingman *et al.*, 2008).

There are two factors that affect the DI of ores in rotary kilns: the tumbling action and the tumbling time. The tumbling effect is associated with three breakage mechanisms: abrasion, attrition, and impact. Abrasion occurs when two particles rub against each other and attrition occurs when two particles (of almost similar size) both rub against one small particle. During tumbling, particles are lifted to the top of the mill and subsequently move perpendicular to the plane of contact, impacting on the other particles and particle-wall contacts; this is therefore referred to as the impact mechanism. These mechanisms are the main causes of fines generation (decrepitation) in rotary kilns. Figure 2 depicts the breakage mechanisms and the zones at which they primarily occur in a rotary kiln. The effect of tumbling time on the amount

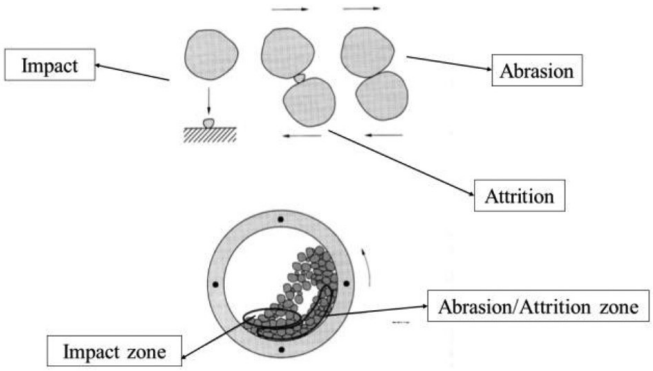

Figure 2—The tumbling action and associated breakage mechanisms (Kingman *et al.*, 2008

Table I

Mineralogy of four types of ores studied by (Faria, Janotti, and da Silva Araújo, 2012)

Mineral composition	Urucum	Morro da mina	Azul	Wessels
Cryptomelane: $K(Mn^{4+}Mn^{2+})_8O_{16}$	>50 %	-	>50%	-
Pyrolusite: MnO_2	<20 %	-	-	-
Braunite: $Mn^{2+}Mn^{3+}{}_6SiO_{12}$	<10 %	-	-	>50 %
Rhodochrosite:$(Mn,Fe,Mg,Ca)CO_3$	-	>50 %	-	-
Spessartine: $Mn^{2+}{}_3Al_2(SiO_4)_3$	-	<50 %	<3 %	-

of fines generated was studied by Kingman *et al.* (2008) using limestone rock samples. The investigation was done for the size fractions of 2.36-3.35 mm, 1.7-1.18 mm, 1.18-1.7 mm, and 0.85-1.18 mm for tumbling durations of 1, 2, 3, 4, 5, 7, 9, and 15 minutes. It was found that increasing the tumbling time increased the mass of fines generated.

The main aim of the research presented here was to determine whether manganese lump ore will decrepitate during preheating in a rotary kiln. The objectives were to determine the effect of temperature, rotational speed, and particle size range on the DIs of three different manganese ores sourced from the Kalahari Manganese Field (KMF) in South Africa.

Methods

A custom-made rotary kiln with a 316 stainless steel rotating tube 78 cm long and inside diameter of 23 cm was used. The kiln is equipped with a REX-P200 temperature controller. The kiln can provide a maximum heating rate of 10°C/min and can reach a maximum temperature of 1 200°C. The kiln is also equipped with a direct current (DC) motor and a variable speed drive which can give a maximum output of 12 r/min. The rotating tube and DC motor are connected by means of gears and chains. For the purpose of these experiments the kiln was kept in a horizontal position.

The ores were supplied by a South African producer of silicomanganese and designated A, B, and C. About 200 kg of each type of ore was utilized for the investigation. The samples were first screened to obtain +6-20 mm, +20-40 mm, and +40-75 mm particle size fractions. Each size fraction was coned and quartered to produce 10 kg samples representative of the batch. The 10 kg samples were then split into 1 kg samples using a rotating splitter.

The 1 kg samples were used for the decrepitation tests or chemical and phase chemical analyses. Inductively coupled plasma optical emission spectrometry (ICP-OES) was used to determine the bulk chemistry and the analyses were done in triplicate. Quantitative X-ray diffraction (QXRD) was applied to determine the bulk modal mineral compositions. A Bruker D8 diffractometer with an acceleration voltage of 35 kV was utilized. A cobalt tube with Fe-low beta filter was used with 2ø angle ranging from 2 to 80 degrees and step size of 0.02°2ø. The samples were then taken for quantitative analysis, using the D-500 diffractometer with Cu Kà radiation and a graphite monochromator. The microstructure and the quantitative elemental analysis of the ores were determined using scanning electron microscope with energy dispersive X-ray spectroscopy (SEM-EDS). This technique utilized a Zeiss Evo MA15 at an acceleration voltage of 20 kV.

The porosity was determined using a He-pycnometer. The pycnometer measures the specific volume of sample placed in the test cup. This value was then used together with the expected volume a particle of unit mass with zero porosity should occupy using Equation [2]. Loss on ignition (LOI) was determined by the ASTM D7348 standard method. Moisture content was determined by the ASTM D2216-19 standard method and bulk density by a modified volumetric method. The modified volumetric method involves filling a hopper of a known mass (with a volume of 4 293 cm³) with ore particles and weighing it. The mass of the empty hopper was subtracted from the mass of the hopper and ore to obtain the mass of the ore. The method was repeated three times. The bulk density was calculated according to Equation [3].

$$X = \frac{A-B}{A} * 100\% \quad [2]$$

where
X = porosity %
A = measured specific volume (g/cm³)
B = expected specific volume (g/cm³)

$$\rho = \frac{M}{V} \quad [3]$$

where
ρ = bulk density (g/cm³)
M = mass of the particles (g)
V = volume of the hopper (cm³)

Temperature (600, 800, or 1000°C) and rotational speed (3, 6 or 12 r/min) setpoints were selected on the controller. The heating rate was kept constant at 2.5 ^{0}C/ min. Once the kiln reached the selected temperature, 1 kg of the ore sample of either the +6-20 mm, +20-40 mm or +40-75 mm size fraction was fed into the kiln using a shovel while it was rotating and held at temperature for 30 minutes. After 30 minutes the sample was allowed to cool and subsequently screened to separate particles <6 mm. The experimental plan for each type of ore is shown in Table II. Parameters marked with (*) are kept constant when investigating the effect of other parameters. For example, when the effect of temperature was investigated rotational speed and size range were kept constant at 6 r/min and +6-20 mm respectively, and temperature was varied from 600 to 1000 ^{0}C.

Results

Characterization of samples prior to heating

The moisture content, porosity, and loss on ignition (LOI) results for the three ores are tabulated in Table III.

The calculated averages of the bulk density measurements of the ore samples, obtained at different size ranges, are presented in Table IV together with the standard deviations calculated. Ore C is denser than the other ores in the study, and the bulk density decreases with increasing size range for all three ores

Table V summarizes the chemical compositions of the ores as determined by ICP-OES. Ore B has the highest manganese (Mn) content followed by ore C and finally ore A. The totals do not sum to 100 because manganese and iron are reported in their metallic forms.

Table II

Experimental conditions which were used for each type of ore

Temperature (°C)	Rotational speed (r/min)	Size range (mm)
600	3	+6-20*
800*	6*	+20-40
1000	12	+40-75

Table III

Moisture content, porosity and LOI for the ores used in the study

Ore type	Moisture content (%)	Porosity (%)	LOI (%)
Ore A	0,83	0,75	6,01
Ore B	0,44	0,71	3,49
Ore C	0,62	0,74	3,61

Table IV

Bulk densities of ores

Ore		Bulk density (g/cm³) +6-20 mm	+20-40 mm	+40-75 mm
A	Average	1.60	1.57	1.53
	Std. dev	0.005	0.002	0.001
B	Average	1.69	1.65	1.63
	Std. dev	0.004	0.001	0.002
C	Average	1.78	1.75	1.72
	Std. dev	0.004	0.003	0.002

The bulk phase chemical compositions of the samples are presented in Table VI. From the table it can be observed that braunite is the main source of manganese in all three ores and that ore A has the highest carbonate content (indicated by kutnohorite, calcite, and dolomite), followed by ore B and then ore C

Figure 3 displays the diffraction patterns for the ore samples. The charts are attached to complement the QXRD iresults in Table VI.

Characterization of samples after heating

The phase chemistry of thermally treated samples of ore A was determined using QXRD analysis, Figure 4 presents the trends for minerals that underwent a change during thermal treatment. It can be observe that heating the sample at 600°C decreased the percentage of braunite from 30% to 24.7%. The braunite content decreases further to 25.7% at 800°C, and then to 6.6% at 1000°C. The hausmannite content was not affected by heating at 600°C, but it then increased from 7.4% to 24.9% at 800°C and to 38.2% at 1000°C. The trials for kutnohorite and dolomite at 600°C are similar to that of hausmannite. These two minerals disappear when the samples are treated at 800°C and 1000°C. The calcite content increases from 20% to 29.3% when treated at 600°C and to 41.4% at 800°C, then drops to 1.5% at 1000°C. The marokite content is zero for untreated material and samples treated at 600°C and 800°C, but then increases to 25% at 1000°C. The content of haematite and bixbyite drops from the initial content when treated at 600°C and then increases to 800°C. But when the samples are treated at 1000°C, the content of bixbyite drops to zero while the content of haematite increases to 11%.

The minerals of ore B that changed during thermal treatment are displayed in Figure 5. There is no difference in braunite content between the untreated sample and the sample treated at 600°C. The braunite content drops from 40% to 35.1% when treated at 800°C and drops further to 12.1% at 1000°C. Hausmannite dropped from 12.3% to 0.8% when treated at 600°C, increased from 0.8% to 23.9% at 800°C and then increased further from 23.9% to 35.7% at 1000°C. The kutnohorite content increased from 10% to 30.7% at 800°C and then dropped to zero at 1000°C. The calcite content drops from the initial 24.4% to 14.7% when treated at 600°C, increases to 32% at 800°C, and then drops again to 2.3% at 1000°C. The trend of haematite drops from 5.5% to 4.4% at 600°C, increases slightly to 4.8% at 800°C, and then increases

Table V

Chemical compositions of Mn ores determined by IPC-OES

Ore		Mn	Fe	Al_2O_3	CaO	MgO	SiO_2	P_2O_5	Total
A	Average	29.24	5.5	0.25	21.51	3.22	4.84	0.06	64.62
	Std. dev	0.23	0.05	0.04	0.15	0.03	0.05	0	
B	Average	38.87	5.16	0.21	15.42	2.01	4.7	0.04	66.41
	Std. dev	0.11	0.04	0.01	0.26	0.01	0.04	0	
C	Average	35.17	4.57	0.21	16.52	2.99	6.01	0.04	65.49
	Std. dev	0.07	0.02	0.01	0.19	0.01	0.04	0	

Table VI

Mineralogical compositions of ores determined by QXRD (mass%)

Mineral	Ideal chemical composition	A	B	C
Haematite	Fe_2O_3	4.5	5.2	-
Jacobsite	$(Fe^{2+})(Mn^{3+})_2O_4$	-	-	6.5
Bixbyite	$(MnFe)_2O_3$	5.4	5.5	-
Braunite	$Mn^{2+}Mn^{3+}{}_6SiO_{12}$	30.2	40.0	29.8
Hausmannite	Mn_3O_4	6.0	12.3	21.3
Kutnohorite	$CaMn(CO_3)_2$	23.2	10.0	14.4
Calcite	$CaCO_3$	20.0	24.6	24.6
Dolomite	$CaMg(CO_3)_2$	9.8	<1	-
Clinopyroxene	$(NaCa)(Mg.Fe.Al)(Al.Si)_2O_6$	-	-	2.7
Jianshuiite	$(Mg.Mn^{2+})Mn^{4+}{}_3O_7.3H_2O$	-	<1	-
	Total	**99.1**	**97.6**	**99.3**

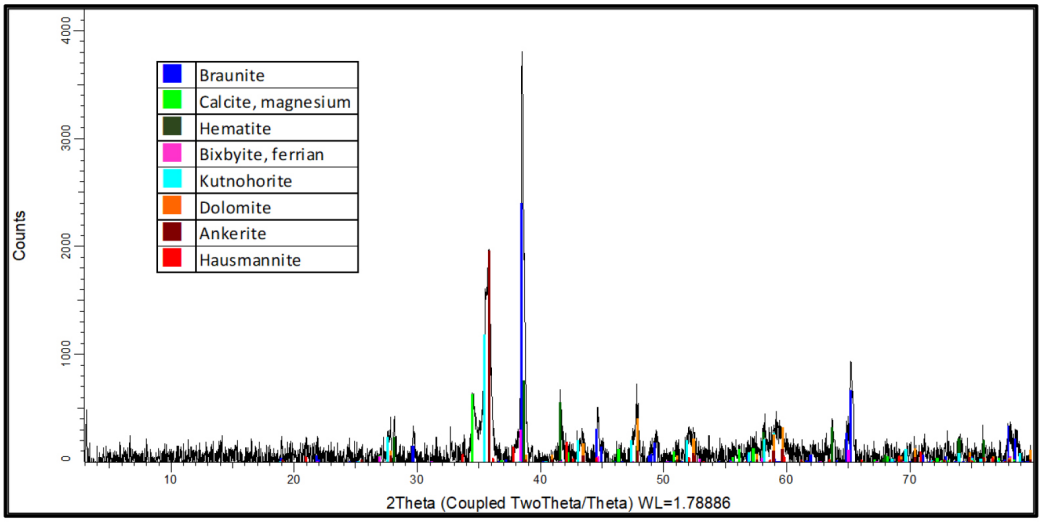

(a)

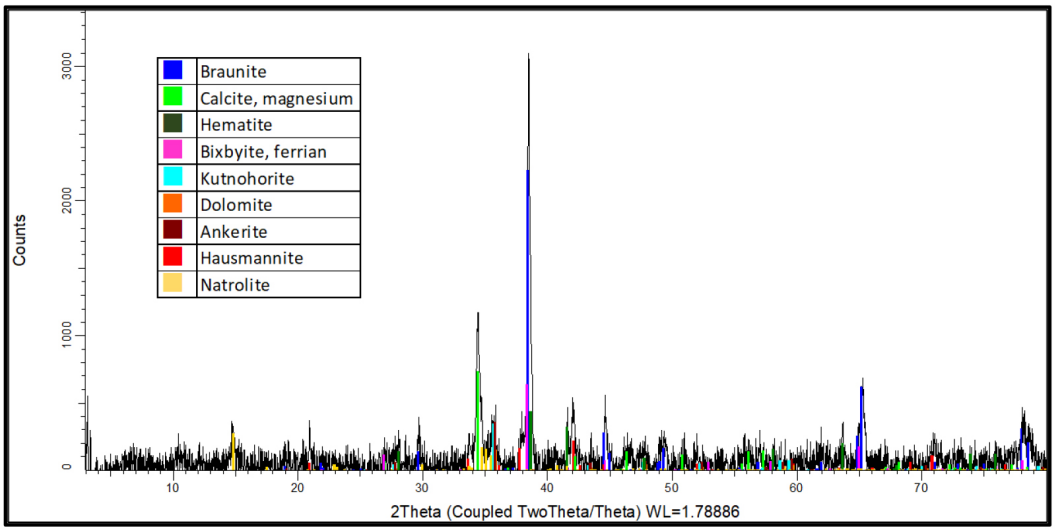

(b)

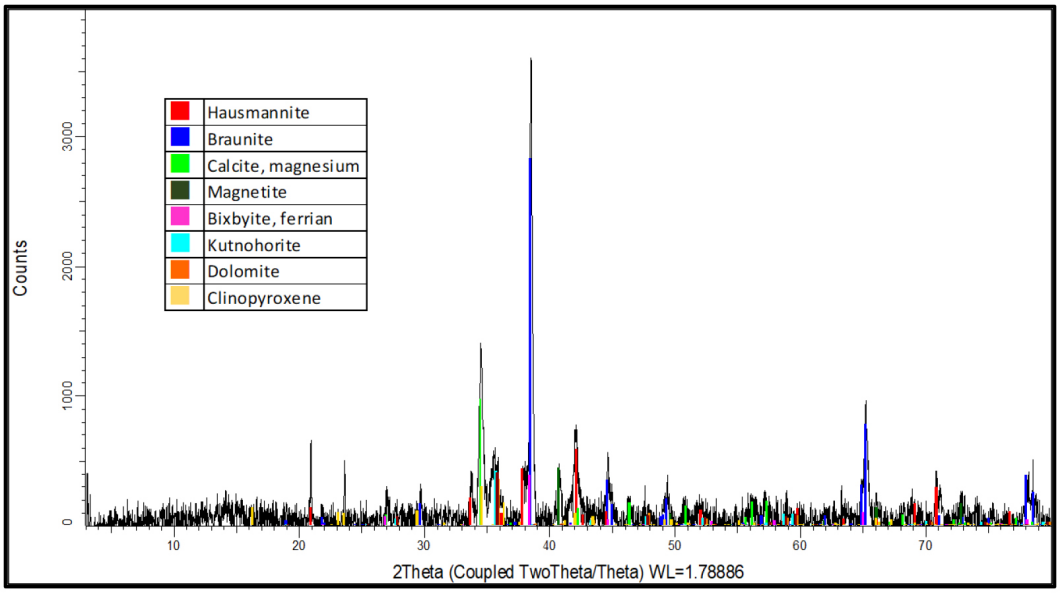

(c)

Figure 3—Diffraction patterns for (a) ore A, (b) ore B, and (c) ore C

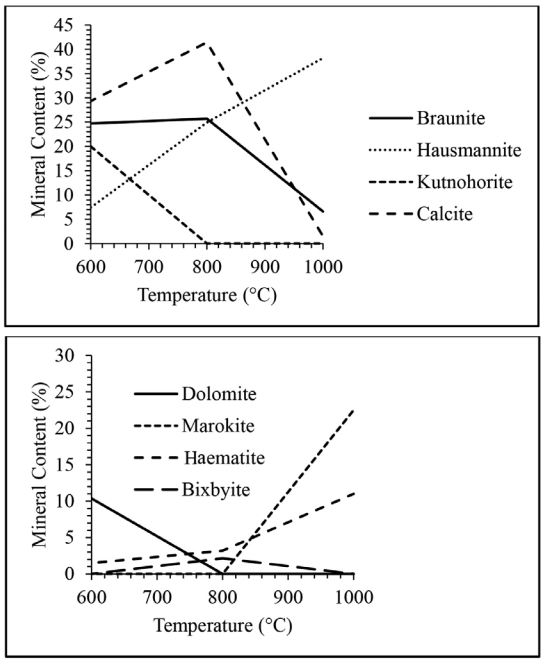

Figure 4—Changes in mineral content of ore A with temperature

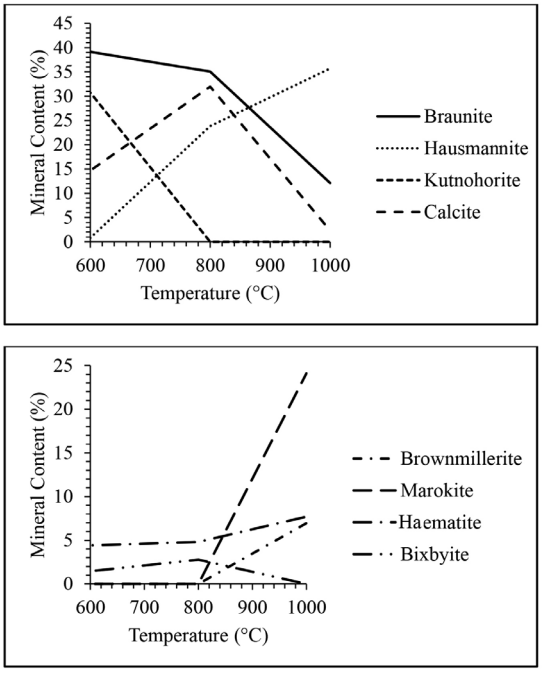

Figure 5—Changes in mineral content of ore B with temperature

from to 7.7% at 1000°C. Bixbyite showed similar trends in ores B and A, starting at 5.5% for untreated samples and dropping to 1.5% at 600°C. The content then increased from 1.5% to 2.8% at 800°C, and dropped tozero at 1000°C.

The change in mineral contents with temperature for Ore C are plotted in Figure 6. Braunite in Ore C and Ore A follows a similar trend: the contents start at 18.3% and increases to 26% when treated at 600°C. The content further increases to 30.4% when treated at 800°C and then drops to 26.8% when treated at 1000°C. The hausmannite content makes a parabolic shape between the temperatures of 600°C and 1000°C, the contents start at 42.9% and drops to 19.3% when treated at 600°C. The percentage then increases from 19.3% to 30.1% when treated

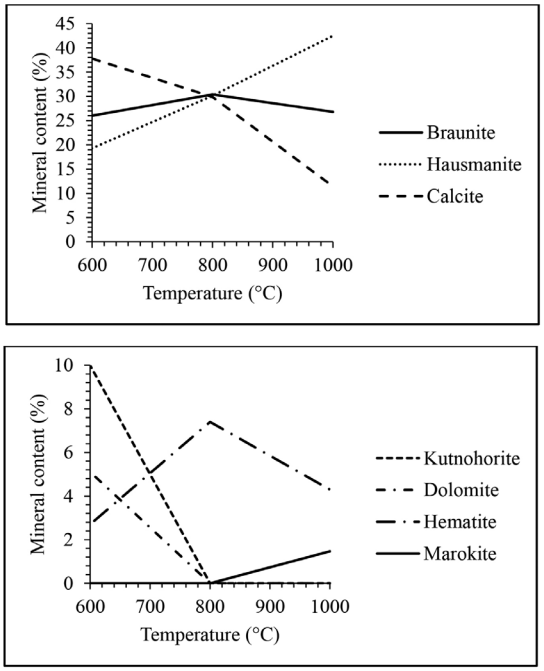

Figure 6—Changes in mineral content of ore C with temperature

at 800°C and then further increases to 42.5% when treated at 1000°C. The content starts at 2% and increases to 37.8% when treated at 600°C and then dropped to 29.9% and 11.4% when treated at 800°C and 1000°C respectively. The kutnohorite content starts at 0% and increases to 10% when treated at 600°C and then drops to 0% when treated at 800°C and 1000°C. Dolomite and kutnohorite follow a similar trend: the content starts at 0% and increases to 5.1% when treated at 600°C and then drops to 0% when treated at 800°C and 1000°C. The hematite content starts at 6% and decreases to 2.7% when treated at 600°C and increases to 7.4% and drops to 4.3% when treated at 800°C and 1000°C respectively. Marokite is only observed when the sample is treated at 1000°C and then at low concentration (1.5%).

Decrepitation index

Figure 7 presents the effect of temperature on the DI of the three ores. Temperature has a significant effect on the DI of all three ores, increasing with temperature. Ore A has the highest DI and ore B the lowest. At 600°C the DI of ore A is 3.6 times that of ore B, while at 1000°C the DI of ore A is 1.3 times that of ore B. However, at 800°C the DI of ore B is 1.21 times that of ore C, while at 1000°C the DI of ore C is 1.08 times that of ore B.

The effect of the rotational speed of the kiln on the DI of all ores is depicted in Figure 8. For ore B and ore C the change in DI is very small when increasing the rotational speed, while for ore A the change is noticeable when moving from 3 r/min to 6 r/min. The effect of rotational speed on the DI is not as significant as the effect of temperature. For this parameter generally ore A has the highest DI followed by ore B and then ore C. At 3 r/min the DI of ore A is only 0.9 times when compared to the DI of ore B, while at 12 r/min the DI of ore A is 1.3 times that of ore B. That is, DI increases with increasing rotational speed although the increase is less pronounced with ore C. The rotational speed has a very little effect on the DI, there being an increase of only 0.85% and 1.22% as the rotational speed increases from 3 to 6 r/min and from 6 to 12 r/min respectively for ore C, while ores A and B increase only slightly more than 2% each time.

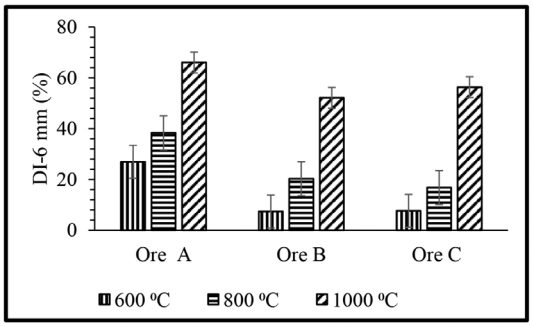

Figure 7—DI of ore A-C at different temperatures (rotational speed 6 r/min size range +6-20 mm)

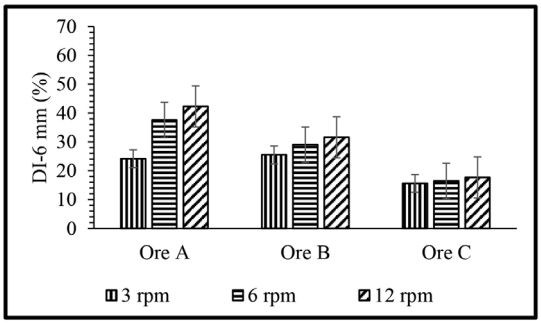

Figure 8—DI of ores A-C at different rotational speed (temperature 800°C, size range +6-20mm)

Figure 9 presents the effect of size range on the DI. This parameter gives rise to opposite trends compared to the effects of temperature and rotational speed. For this parameter ore B has the highest DI followed by ore A and then ore C. The DI decreases with increasing size range. The effect is the greatest for ore B and small for the other ores. For a size range of +6-20 mm the DI of ore B is 1.1 times that of ore A, while for a size range of +40-75 mm the DI of ore B is only 0.8 times that of ore A.

Discussion

Effect of temperature

Figure 7 shows the effect of temperature on the decrepitation index of manganese ores. As shown by the changes in mineral content for ore A in (Figure 4), kutnohorite decreased during thermal treatment and dropped to zero at 800°C. This drop is due to the decomposition of kutnohorite, at 500°C as shown in Equations [3] and [4] (Faria *et al*, 2010, 2012, 2013). This decomposition process explains why the trend of DI for these three ores followed the kutnohorite content in the untreated samples. Braunite transforms into hausmannite (Mn_2O_4) at a temperature of 700°C or higher (Faria, Jannoti, and da Silva Araújo, 2012). This transformation of braunite to hausmannite also contributes to increasing the DI in the ores treated at 800°C and 1000°C. Faria *et al*., (2010) concluded that phase transformation is one of the reasons decrepitation occurs, therefore this finding is in agreement with the literature. It was mentioned in the literature review that a change in crystalline structure induces stress that causes cracks during phase transformation and contributes to decrepitation (Faria, Jannoti, and da Silva Araújo, 2012). As shown in Figure 10, the sample treated at elevated temperature (1000°C) has more cracks per unit area than the sample treated at low temperature (600°C). Although braunite and hausmannite both have a tetragonal

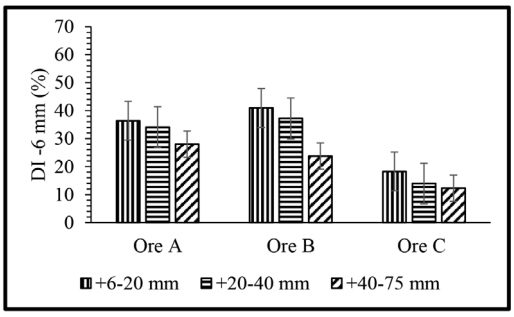

Figure 9—DI of ores A-C at different size ranges (temperature at 800°C, rotational speed 6 r/min)

crystallite structure, hausmannite has a tetragonal distorted spinel structure (Benardini *et al*., 2020; Bevan and Martin., 2008). Because hausmannite has a distorted structure and braunite does not, the stress induced during phase transformation caused cracking and contributed to an increase in DI. The chemical composition of the dark and light areas in the SEM images are displayed in Table VII.

$$CaMn(CO_3)_2 \rightarrow CaCO_3 + MnO + CO_2 \quad [4]$$

$$CaCO_3 \rightarrow CaO + CO_2 \quad [5]$$

Moisture content and LOI of the ores also play a role in decrepitation (Dollimore *et al*., 1994; Faria *et al*., 2013). From Table III the trends for moisture content and LOI are similar to the trends for DI. Ore A has the highest moisture content and LOI as well as DI, followed by ore C and finally ore B. From the literature it is seen that ores with a higher moisture content decrepitate more, because heating water raises its vapour pressure (Faria *et al*., 2013, 2012, 2010). Should the moisture be trapped in the inner pores, the vapour pressure can rise high enough to cause rupture and breaking of the ore particle. Fracture of ore particles with closed pores is possible when heated to high temperatures. (Faria, Jannoti, and da Silva Araújo, 2012). This is also one of the reasons why the samples treated at a higher temperature (1000°C) have a higher DI than those treated at lower temperature (600°C). This finding is also in agreement with the literature (Faria *et al*.,2013). LOI is typically seen as the amount of volatile material available in a soil or ore sample. As seen from the experiments conducted at higher temperatures and the changes in bulk phase chemical compositions observed, LOI is a useful standardized test to conduct to give an indication of the carbonate content of the ore.

Studies by Faria *et al.* (2010, 2012, and 2013) indicated that manganese-bearing carbonate minerals such as kutnohorite start to decompose at a temperature of 500°C, which explains why kutnohorite decreased during heat treatment. The ore that has the highest kutnohorite content (ore A) also had the highest decrepitation index. This indicates that the presence of kutnohorite greatly influences decrepitation. Braunite transforms into hausmannite at a temperature of 700°C and higher and this explains the increase of hausmannite content found in this study (Faria, Jannoti, and da Silva Araújo, 2012). Since 600°C is below the transformation temperature of 700°C, this also explains why the increase in hausmannite at 600°C is small compared to the increase when the sample is treated at 800°C. The phase change of these minerals is one of the reasons we have a DI of 26.97% (ore A at 600°C and 6 r/min). Faria *et al*., (2010) concluded that phase transformation is one of the reasons decrepitation occurs, therefore this finding is in agreement with literature.

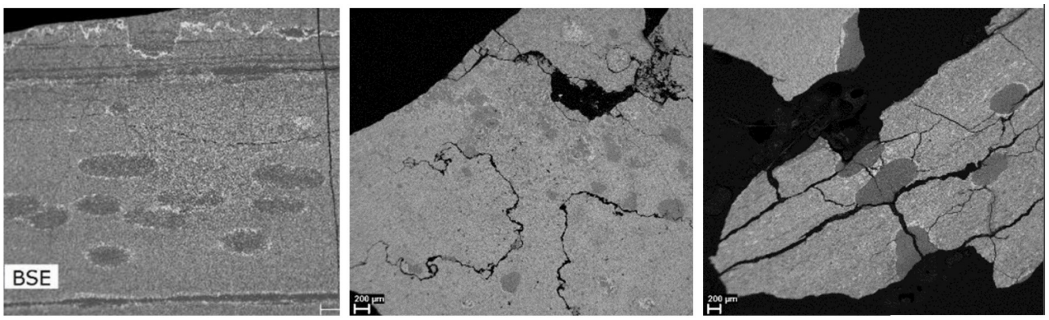

Figure 10—SEM images showing formation of cracks in ore A samples treated at (a) 600°C, (b) 800°C, and (c) 1000°C at 6 r/min and size range of +6-20 mm

Effect of rotational speed

The effect of rotational speed on the decrepitation index of manganese ores is shown in Figure 8. From the literature, it has already been established that decrepitation in a rotary kiln is also influenced by the mechanical breakage which is brought about by the rotation (Kingman *et al*., 2008). This breakage involves three mechanisms attrition, abrasion, and impact (Figure 2). Increasing the rotational speed increases the intensity of these breakage mechanism, resulting in an increase in DI. The kiln had a critical speed of approximately 85.6 r/min, which is seven times more than the highest rotational speed used in the tests. In addition, Faria and co-worker showed that the porosity of the ore may affect the DI, such that an increase in ore porosity increases the DI. The understanding is that an ore with high porosity is much more likely to break under impact. This further explains the higher DI for ore A, and lower DI for ore B and ore C. The other factor that affects the DI of the ores when the rotational speed is adjusted, is the frequency at which the ore particles collide with each other and with the walls of the kiln. Interparticle collisions cause, the particles to break due either to attrition or abrasion (Kingman *et al*., 2008). When the particles collide with the walls of the kiln tube, they break due to impact damage (Kingman *et al*., 2008). When the kiln rotates at a higher speed, the particles in the kiln also move at a higher speed, which increases the frequency of collision between the particles and the walls of the tube. Hence the DI increased when the rotational speed was increased from 3 to 6 and then to 12 r/min.

Effect of size range

The effect of size range on the DI of manganese ores is shown in Figure 9. Since for all the experiments 1 kg of sample was used, it can be assumed that the number of particles decreases with increasing size range. This decreases the probability of interparticle collision, which in turn reduces the DI. Another factor that affects the DI of the ores is the area of contact between the particles when the abrasion breakage mechanism applies. Therefore, when the ore particles are large, the voidage between them is greater which results in small area of contact between particles. Lower bulk density essentially means more total space between the particles (voidage) and a smaller area of contact between the particles of the same ore type. This leads to a reduced formation of fines and ultimately a lower DI at larger size ranges.

Conclusion

The aim of the research was to investigate the of decrepitation of three South African manganese ores in a rotary kiln preheating unit. The decrepitation index (DI) of each ore was measured based on three process parameters, namely temperature, rotational speed, and ore size range. The following conclusions were drawn from the results of the study.

- Increasing temperature increased the DI for all three ores. Ore A was found to have a higher DI than the other two ores. Ore B was the least susceptible to decrepitation. The DI of ore A increased from 26.97% to 38.36% and from 38.36% to 65.99% when the temperature was increased from 600°C to 800°C and from 800°C to 1000°C. The DI of ore B increased from 7.41% to 20.31% and from 20.31% to 52.15% when the temperature was increased as above, and the DI of ore C increased from 7.68% to 16.80% and then to 56.34%.
- Increasing rotational speed increased the DI for all three ores, although the effect was not as significant as that of temperature. Ore A was the most affected by rotational speed, and Ore C the least. The DI of ore A increased from 24.15% to 37.57% and from 37.57% to 42.31% when the speed was increased from 3 r/min to 6 r/min and from 6 r/min to 12 r/min respectively. The DI for ore B increased from 25.48% to 29.02% and from 29.02% to 31.58%, and the DI of ore C from 15.62% to 16.47% and from 16.47% to 17.69%.
- Increasing the size range of the sample decreased the DI. The effect of size range on DI was also not as significant as the effect of temperature. Ore B was the most susceptible in this regard, followed by ore A and finally ore C. The DI of ore A decreased from 36.41% to 34.11% and from 34.11% to 28.03% when the size range was increased from +6-20 mm to +20-40 mm and from +20-40 mm to +40-75 mm respectively. The DI for ore B decreased from 40.99% to 37.23% and from 37.23% to 23.77%, and that of ore C from 18.27% to 13.95% and from 13.95% to 12.30%.

In summary, increasing the temperature and the rotational speed of the kiln increases the DI for all three ores. Increasing the size range of the sample used for the test decreases the DI for all three ores. For further study it is recommended that the effects of heating rate and heating time as well as the gas atmosphere on the DI be investigated.

Acknowledgements

The PREMA project is thanked for providing funds that made the execution of the project possible. The PREMA project is funded by the European Union's Horizon 2020 Research and Innovation Programme under Grant Agreement No. 820561 and industry partners Transalloys, Eramet, Ferroglobe, OFZ, and Outotec.

Mintek and Transalloys provided equipment and the raw material used throughout the project. The paper is published with permission of Mintek.

References

ASTM D2216. 2014. Standard Test Methods for Laboratory Determination of Water (Moisture) Content of Soil and Rock by Mass. ASTM International, West Conshohodcen, PA.

ASTM D4892. 2008. Standard Test Method for Density of Solid Pitch (Helium Pycnometer Method). ASTM International, West Conshohodcen, PA.

ASTM D7348. 2008. Standard Test Methods for Loss on Ignition (LOI) of Solid Combustion Residues. ASTM International, West Conshohodcen, PA.

Benardini, S., Bellatreccia, F., Della Vetura, G., Ballirano, P., and Sodo, A. 2020. Raman spectroscopy and laser-induced degradation of groutellite and ramsdellite, two cathode materials of technological interest. *RSC Advances*, vol. 10. 923 p.

Bevan, D.J.M. and Martin, R.L. 2008. The role of the coordination defect: A new structural description of four fluorite-related sesquioxide minerals, bixbyite, braunite, braunite II, parwelite, and their structural relationships. *Journal of Solid State Chemistry*, vol. 181. pp. 2250–2259.

Biswas, A., Das, P.K., and Singh, V. 2016. Investigation of the decrepitation phenomenon of polymorphic materials: A theoretical and experimental study. *Powder Technology*, vol. 294. https://doi.org/10.1016/j.powtec.2016.02.020

Dollimore, D., Dunn, J.G., Lee, Y.F., and Penrod, B.M. 1994. Decrepitation of dolomite and limestone. *Thermochimca Acta*, vol. 273. https://doi.org/10.1021/a19600006p

Faria, G.L., Jannoti, N., and da Silva Araujo, F.G. 2012. Decrepitation behavior of manganese lump ores. *International Journal of Mineral Processing*, vol. 102. https://doi.org/10.1016/j.minpro.2011.10.004

Faria, G.L., Tenório, J.A.S., Jannotti Jr, N., and da Silva Araújo, F.G. 2013. Disintegration on heating of a Brazilian manganese lump ore. *International Journal of Mineral Processing*, vol. 121. https://doi.org/10.1016/j.minpro.2013.06.008

Faria, G.L., Vianna, N.C.S., Jannoti, N., Vieira, C.B., and Da Silva Araujo, F.G. 2010. Decrepitation of Brazilian manganese lump ores. *Proceedings of the International Ferroalloys Congress*, Helenski, Finland, 6–9 June 2010. pp. 449–455.

Kingman, S.W., Lowndes, I.S., Petavratzi, E., and Whittles, N. 2008. An investigation into the mechanism of dust deneration in a tumbling mill. *Journal of Rock Mechanics and Tunnelling Technology*, vol. 14, no. 26. pp. 77–102.

Olsen, S.E., Tangstad, M., and Lindstad, T. 2007. Production of Manganese Ferroalloys. Tapir Academic Press, Trondheim, Norway.

Pegels, A. 2010. Renewable energy in South Africa: Potentials, barriers and options for support. *Energy Policy*, vol. 38, no. 9. pp. 4945–4954. https://doi.org/10.1016/j.enpol.2010.03.077

Pisaroni, M., Sadi, R., and Lahaye, D. 2012. Counteracting ring formation in rotary kilns. *Journal of Mathematics in Industry*, vol. 19. https://doi.org/10.1186/2190-5983-2-3

PREMA. 2019. https://www.spire2030.eu/PREMA [accessed 20 February 2019].

Sangine, E. 2020. Mineral commodity summaries 2020. US Geological Survey. https://doi.org/10.3133/mcs2020 ◆

ESGS ENVIRONMENTAL SOCIAL GOVERNANCE SUSTAINABILITY
SAIMM COMMITTEE
THE SOUTHERN AFRICAN INSTITUTE OF MINING AND METALLURGY

The Just Transition and the Coal Mining Sector in South Africa

Megan Cole, Mzila Mthenjane, and Andrew van Zyl

Growing concern over the impacts of climate change across the world has led to the widely-shared goal of a 'just transition' to cleaner energy sources and reduced dependence on coal. Different definitions are used for the just transition, but a key feature is that no-one is left behind when changes are made to energy and economic systems to mitigate climate change. That involves sharing the costs and benefits of the changes fairly, supporting workers with new jobs or retraining, and supporting communities through broader economic changes. Crucial to the just transition is preventing further societal fragmentation along wealth, race, age, and gender lines.

Internationally, there has been a transition away from coal mining, particularly in Europe, and a growing awareness of the need for new policies to address job losses, skills shortages and changing value chains and supply chains. South Africa is under pressure to do the same, as the world's seventh largest coal producer and the fourteenth biggest CO_2 emitter. In addition, South Africa is going to experience greater temperature increases than the global average and adaptation to climate change is a growing concern.

There are 72 operating coal mines in South Africa, largely in Mpumalanga Province, supplying the domestic and export markets. They are owned by 32 mining companies who directly employ over 92 000 people and support approximately 170 000 jobs indirectly. According to available life-of-mine data, at least 17 of these mines could close by 2030 (total production of 33 Mt/a), a further 22 mines by 2040 (100 Mt/a), and 13 mines (47 Mt/a) by 2050 (Figure 1). They supply coal to 15 Eskom power stations, which employ over 12 000 people. Most of these power stations are pushing the limits of their design life, and six of them will be decommissioned by 2030 (9.3 GW), a further four by 2040 (14 GW), and three more by 2050 (12.3 GW). New coal-based power projects, when considered in the light of the cost and time overruns of Kusile and Medupi, would not come on stream fast enough to prevent severe energy shortages even if financing was available and there were no climate considerations in play.

This indicates a clear path to decarbonization and means that the transition away from coal to renewable energy is already planned and will likely occur without premature closure implied by the 'just transition'. In fact, mining companies are contributing to the transition by installing their own renewable energy solutions at mine sites, with a commitment of 6.5 GW by 29 companies across various commodities planned to date. This approach is a shared and responsible pathway to the energy transition given our domestic energy and economic challenges. Despite ambitious commitments to low carbon growth, political and governance factors have hindered the rollout of renewable energy. However, renewable projects that have proceeded have performed well and there is some cause for optimism now that regulatory progress has been made. Further research may also show that employment in the energy sector in a renewable energy dominant economy may be higher.

The Just Transition and the Coal Mining Sector in South Africa *(continued)*

The impact of mine closure on host communities is significant, disruptive, and should not be underestimated. Coal mines currently operate in two metros and 21 local municipalities, home to over 10 million people. Specifically, there are at least 50 coal mining host communities (4 cities, 24 towns, 14 townships, and 8 rural villages) that are home to 2.5 million people. These communities already have low levels of employment (39% unemployed), income (37% below the poverty line), education (45% of adults have Grade 12/NQF4), and internet access (Figure 2) and thus are vulnerable to a changing energy system and local economy. The level of basic services varies significantly but is lowest in rural areas with the lowest income levels and fewest job opportunities. Importantly, many of the local municipalities are under financial stress and will struggle to cope with mine closure and the resultant loss of revenue and support.

The South African approach to the 'just transition' needs to take into account these local realities and the narrative needs to support an effective transition that does not undermine the economy or the social licence to operate of the coal mines that are currently an essential part of the energy system. Much work has already been done on stakeholder engagement, but clarity is needed on the drivers and nature of the transition, which in reality is a planned socio-economic transition to closure, in addition to environmental considerations.

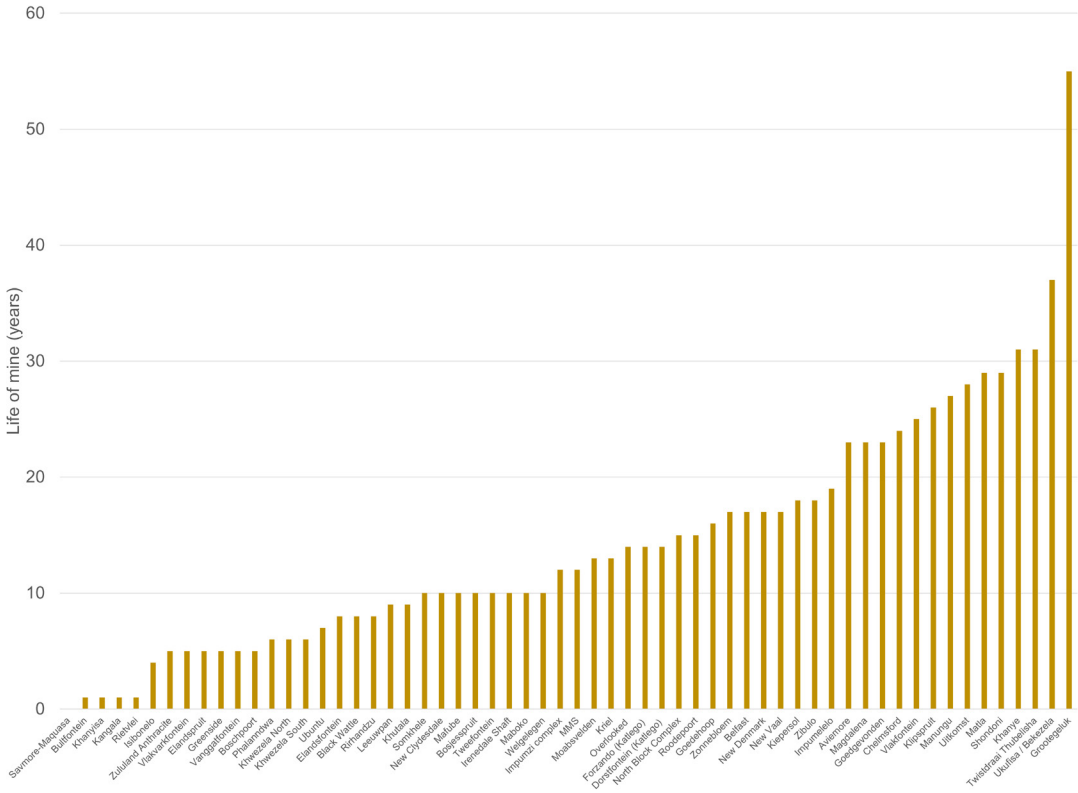

Figure 1 – Life-of-mine of coal mines in South Africa

Figure 2 – Social wellbeing barometer for coal mining host communities in South Africa